Annual carbon emissions from land-use change in China from 1000 to 2019

Fan Yang[1,2], Guanpeng Dong[1,2], Xiaoyu Meng[1,2], Richard A. Houghton[3], Yang Gao[1,2], Fanneng He[4], Meijiao Li[5], Wenjin Li[1], Zhihao Liu[1], Xudong Zhai[1], Pengfei Wu[1], Hongjuan Zhang[1,2], Qinqin Mao[6], Yuanzhi Yao[7], Chao Yue[8]

[1]Key Research Institute of Yellow River Civilization and Sustainable Development, Henan University, Kaifeng 475001, China

[2]Laboratory of Climate Change Mitigation and Carbon Neutrality, Henan University, Zhengzhou 475001, China

[3]Woodwell Climate Research Center, Falmouth, MA 02540, USA

[4]Key Laboratory of Land Surface Pattern and Simulation, Institute of Geographic Sciences and Natural Resources Research, Chinese Academy of Sciences, Beijing 100101, China

[5]College of Resources and Environment, Shanxi University of Finance and Economics, Taiyuan 030006, China

[6]Piesat Information Technology Co., Ltd., Xian, 710100, China

[7]School of Geographic Science, East China Normal University, Shanghai, 200241, China

[8]College of Natural Resources and Environment, Northwest Agriculture and Forestry University, Yangling 712100, China

Correspondence to: Guanpeng Dong (gpdong@vip.henu.edu.cn), Fanneng He (hefn@igsnrr.ac.cn), and Chao Yue (chaoyue@ms.iswc.ac.cn)

Abstract. Long-term land-use changes have profound impact on terrestrial ecosystem and the associated carbon balance. Current estimates of China's historical carbon emissions induced by land-use change varies widely, where in the magnitude of China for 1950–2021 exhibit great uncertainties reaching as large as 150% in global estimates, while the national-scale estimates for a longer time period of past 300 years show a relative uncertainty of 102%. Here, we utilized bookkeeping method to quantify China's annual carbon budget resulting from land-use change between 1000 and 2019, driven by a millennial dataset of land-use change in China in provincial level, assisted with comprehensive soil and vegetation carbon density datasets. This approach, supported by high-confidence land-use change data, extensive soil and vegetation carbon field sampling, and an updated disturbance-response curve, enhanced the accuracy of carbon budget estimations. The results revealed that cumulative carbon emissions from land-use change in China reached 19.61 Pg C over the past millennium. Moreover, critical turning points occurred in the early 18th century and early 1980s, with emissions accelerating in the 18th century and transitioning from carbon source to carbon sink in the early 1980s. Our findings revealed values 68%–328% higher than previous 300-year estimates, suggesting that historical carbon emissions from land-use change in China may have been significantly underestimated. This study provides a robust historical baseline for assessing terrestrial ecosystem carbon budgets at national and provincial scales, both in the present and future. The dataset is available at https://doi.org/10.5281/zenodo.14557386 (Yang et al., 2025).

1 Introduction

Carbon fluxes from historical and current land-use change, including both gross emission and sinks but globally as a net carbon source, are a critical component of the global carbon budget (Houghton and Nassikas, 2017). On the other hand, reversing land use practices that cause emissions can provide insights into the potential of land management to remove carbon from the atmosphere. Improved quantification of the carbon dynamics associated with land-use change is hence needed to provide a better understanding of the global carbon cycle and the future carbon sink potential of terrestrial ecosystems (Friedlingstein et al., 2023; Obermeier et al., 2024).

Although the estimated contemporary carbon emissions from land-use change account for only 10–15% of anthropogenic carbon emissions (Friedlingstein et al., 2022; Friedlingstein et al., 2020), their contributions were much higher in the past. Land-use change has been estimated to contribute nearly 20 ppm to current atmospheric CO_2 concentrations, with this contribution dating back at least 1,000 years (Pongratz et al., 2009). Over the past 150 years, carbon emissions from land-use change have accounted for up to 33% of global anthropogenic carbon emissions (Houghton et al., 2012). Recent consistent carbon accounting shows that since 1750, land-use change has been a major source of CO_2 emissions, accounting for 54% of the cumulative CO_2 emissions from 1750 to 2020, with fossil fuel CO_2 emissions not surpassing those from land-use change until the mid-1960s (Dorgeist et al., 2024; Wedderburn-Bisshop, 2024). Furthermore, historical carbon emissions from land-use change provide crucial insights into how the global carbon cycle responds to environmental changes (Houghton and Castanho, 2023; Yue et al., 2020; Houghton and Nassikas, 2017).

Given the profound impact of land-use change, particularly over long timescales, numerous studies have focused on long-term global estimates of carbon emissions from land-use change (Houghton and Castanho, 2023; Mendelsohn and Sohngen, 2019; Houghton and Nassikas, 2017; Kaplan et al., 2011; Pongratz et al., 2009). However, uncertainties persist in these estimates (Winkler et al., 2023), with net land-use change carbon fluxes exhibiting the highest relative uncertainty in global carbon budget (GCB) assessments (Friedlingstein et al., 2022). These uncertainties arise not only from differences in estimation models, parameters, and carbon density datasets but also from historical land-use change data. In particular, reliable land-use change datasets prior to the mid-20th century are often lacking for many countries, including China.

On typical approach to reconstructing historical land use change is to use historical population data as proxies combined linear backcasting (Pongratz et al., 2008; Klein Goldewijk, 2001; Ramankutty and Foley, 1999). Although this method works reasonably well for estimating cropland and pasture areas, it is less suitable for calculating changes in forest cover, which has high impact on estimated terrestrial ecosystem carbon budgets because of the higher carbon densities often found in forest ecosystems than cropland or grassland. As a result, researchers often subtract the area of cropland and pasture from the potential natural vegetation to estimate forest cover change (Hurtt et al., 2020; Klein Goldewijk et al., 2017; Pongratz et al., 2008; Ramankutty and Foley, 1999). However, this approach fails to capture large-scale forest cover change driven by

factors such as shift cultivation, timber and fuel demand in addition to land conversion for agriculture. Consequently, this

65   indirect method can only reflect the conversion relationship among forests, croplands, and pastures, often resulting in underestimates of the actual extent of historical forest change. Therefore, whether linear backcasting or potential vegetation subtraction is used, great uncertainties are often introduced by these methods (Kabora et al., 2024; Yang et al., 2020; He et al., 2018), which are carried over into land-use carbon emission estimates.

China has vast territory and a long history of land use, making it an important contributor to global terrestrial carbon

70   dynamics caused by anthropogenic land use change and land management. Additionally, China has abundant historical documentation, such as tax records for cropland areas from a number of dynasties. Scholars have used these records to reconstruct long-term, high-confidence, datasets of cropland areas, thereby providing a strong foundation for estimating historical land-use change carbon emissions. Previous studies have extensively reconstructed historical land use across China and specific regions (He et al., 2023; Jia et al., 2023; Wei et al., 2022; Yang et al., 2022; Yu et al., 2021; Li et al., 2016; Ye et

75   al., 2009), as well as the associated carbon emissions (Yang et al., 2023; Yu et al., 2022; Yang et al., 2019; Li et al., 2014; Ge et al., 2008; Houghton and Hackler, 2003). However, existing estimates vary widely and exhibit great uncertainty. For example, estimates of cumulative net carbon emissions from land-use change in China from 1950 to 2021 based on three internationally recognize bookkeeping models exhibited a relative uncertainty of up to 150% (ratio of the standard deviation to the mean estimate) (Obermeier et al., 2024). Moreover, independent estimates of carbon emissions from land-use change

80   over the past 300 years for China also showed a relative uncertainty of 102% (Yang et al., 2023; Yang et al., 2019; Ge et al., 2008; Houghton and Hackler, 2003). Although uncertainty can be reduced by improving model selection and parameters, highly reliable land-use change data remain crucial (Dorgeist et al., 2024; Yu et al., 2022).

To address these issues, this study combined several locally reconstructed, high-confidence, long-term land use change datasets with comprehensive carbon density datasets to estimate carbon emissions from land use change for 1000–2019 in

85   China. First, we extended the analysis period from 1700 to 1980 to 1000 to 2019 using newly published millennial land-use change reconstruction data for China (He et al., 2023; He et al., 2024) in combination with data from the Second and Third National Land Surveys in China. This update also improves the reliability of the data, thus providing more confident historical land-use change trajectories and effectively reducing the uncertainty in carbon budget estimates. Second, we developed new land-use conversion rules that clarify the attribution of deforestation beyond conversion to cropland, which is

90   an essential component for calculating annual land-use change rates. Third, carbon density sampling data were enriched to enhance their representativeness. Finally, an improved bookkeeping model with an updated disturbance-response curve was used to calculate the annual carbon fluxes associated with long-term land-use change in China. This method represents a key approach used by both the IPCC and Global Carbon Project (GCP) to estimate carbon emission fluxes from land-use change.

2. Material and methods

2.1 Study area

China's territorial and administrative boundaries have changed frequently over the past millennium, with the country experiencing a succession of different regimes, including the Liao, Song, Jin, Yuan, Ming, and Qing dynasties, Republic of China, and People's Republic of China (Figs. 1a–e). To facilitate the alignment of data across different historical periods, this study used the current land area of China as the study region. The territorial and administrative coordination scheme proposed by He et al. (2023) at the provincial level were adopted as the basic unit for analysis (Fig. 1f). This coordination scheme also serves as a fundamental unit for historical land-use change data in China (cropland, forest, and grassland).
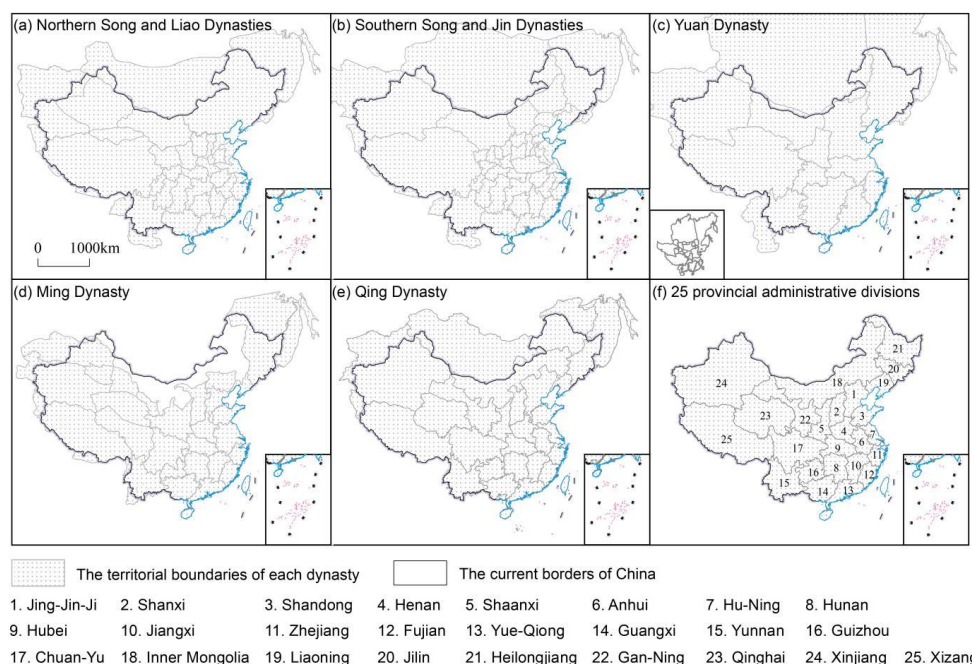

Figure 1. Territorial changes across dynasties and the 25 merged provincial-level administrative divisions of China. Some provincial-level administrative regions have been merged: Beijing, Tianjin, and Hebei were merged into JingJin-Ji (No.1); Shanghai and Jiangsu were merged into Hu-Ning (No.7); Guangdong and Hainan were merged into Yue-Qiong (No.13); Sichuan and Chongqing were merged into Chuan-Yu (No.17); and Gansu and Ningxia were merged into Gan-Ning (No.22). Due to data limitations, this study did not include Taiwan Province.

2.2 Data sources

This study used two main types of data: long-term land-use data (cropland, forest, and grassland) and carbon density data (vegetation carbon density and soil carbon density).

2.2.1 Land-use data

Land-use data for the period 1000–2019, covering 131 time points, included both historical reconstruction data and

115 survey-based statistics. For the period 1000–1999, provincial cropland data for China were obtained from several previous

studies (Table 1). These data were primarily reconstructed for cropland areas using tax records in historical archives dating

back to the Northern Song Dynasty (Yang et al., 2024; Li et al., 2020; Li et al., 2018a; Li et al., 2018b; Li et al., 2016; Ge et

al., 2004). Provincial forest data for 1000–1998 were sourced from He et al. (2024, 2017, 2008) (Table 1) and are referred to

as historical deforestation data. Provincial grassland data for 1000–2000 were also obtained from He et al. (2024) (Table 1).

120

Table 1. Data sources for land-use change in China

Data variables	Temporal coverage	Spatial resolution	Data type	Data source/ Reference
Cropland	1000, 1066, 1078, 1162, 1215	Province	Reconstruction	He et al. (2017); Li et al. (2018a)
	1102	Province	Reconstruction	Yang et al. (2024)
	1290	Province	Reconstruction	Li et al. (2018b)
	1393, 1583, 1620	Province	Reconstruction	Li et al. (2020)
	1661–1949 (21 time points)	Province	Reconstruction	Ge et al. (2004)
	1949–1999 (27 time points)	Province	Statistics	Li et al. (2016)
Forest	1000–1949 (50-year interval)	Province	Reconstruction	He et al (2024) He et al (2008)
	1962, 1976, 1981, 1988, 1993, 1998	Province	Statistics	He et al (2015)
Grassland	1000, 1100, 1200, 1300, 1400, 1500, 1600, 1700, 1800, 1900, 2000	Province	Reconstruction	He et al (2024)

This study used survey-based data from the Second National Land Survey (2009) and Third National Land Survey (2019)

(Appendix Table A1) for the period after 2000. These surveys, conducted by the Chinese government, are considered highly

125 credible.

The 25 provinces shown in Figure 1 were used as spatial units for historical land-use data in China (Fig. 1). Cropland,

forest, and grassland data from the national land survey reports were adjusted according to this scheme to ensure consistency.

2.2.2 Carbon density data

This study constructed a provincial vegetation and soil carbon density dataset for China based on 10,424 vegetation and soil

130 carbon density sample points. Soil carbon density data were derived from the following three sources. (1) The 2010s China

Land Ecosystem Carbon Density Dataset (Xu et al., 2019). This dataset consolidates field measurement data from 2004 to

2014 reported in publicly available literature. From this dataset, 1,235 sample points for forest soil carbon density and 614

sample points for grassland soil carbon density were extracted. (2) The Second National Soil Survey of China (1979–1985).

This survey resulted in the publication of the Soil Chronicles Atlas of China, Volumes 1–6, which record soil property data

135   from the 1980s. From this, 339 sample points for forest soil properties and 147 sample points for grassland soil properties

were extracted. (3) The Chinese Soil Series (since 2008). This investigation produced the Soil Series Atlas of China, which

consists of 30 volumes (Appendix Table B1). From this dataset, 724 and 529 sample points for forest and grassland soil

properties were extracted, respectively. The spatial distribution of the sample points is presented in Appendix Fig. B1.

The results of the two large-scale soil surveys were documented in books that recorded soil properties during different

140   periods in China. This study extracted information from these surveys, including the geographic location (latitude and

longitude), soil depth (0–100 cm), soil type, organic carbon content, soil bulk density, and >2 mm gravel content, and applied

Eq. (1) to calculate the soil carbon density. The formula used to calculate soil carbon density based on soil properties is as

follows:

$$C_S = \sum_{i=1}^{n} SOC_i \times D_i \times BD_i \times (1 - SC_i) \times 0.1 \tag{1}$$

where C_S is the soil organic carbon density, SOC_i is the organic carbon percentage in the i-th soil layer (%), D_i is the

145   thickness of the i-th soil layer (cm), BD_i is the bulk density of the i-th soil layer (g/cm³), SC_i is the percentage of gravel

(>2mm) in the i-th soil layer (%), and n is the number of layers in the 100 cm soil profile. This study only selected sample

points with a soil profile thickness of $\geq$ 100 cm but only the carbon density within the top 100 cm was considered. For

sample points lacking bulk density data, bulk density was estimated using a transfer function (Yang et al., 2007).

Vegetation biomass carbon density data were sourced from the 2010s China Land Ecosystem Carbon Density Dataset (Xu

150   et al., 2019), including both aboveground (forests: 1,610 points, grasslands: 2,224 points) and belowground (forests: 1,544

points, grasslands: 1,458 points) carbon density data from both forest and grassland ecosystems. The formula for calculating

vegetation carbon density is as follows:

$$C_v = C_{above\_ground} + C_{below\_ground} \tag{2}$$

where C_v is the vegetation biomass carbon density, C_{above_ground} is the aboveground vegetation carbon density, and C_{below_ground}

is the belowground vegetation carbon density.

155   The collected vegetation biomass and soil carbon density data were grouped according to the 25 merged province-level

administrative divisions described above based on the geographic coordinates of the data points. Overall, for each province,

the sample points exhibited a normal distribution (Appendix Figs. B2–B4). The arithmetic mean was used to calculate the

provincial-level average carbon density. For provinces with exceptionally high or low values, the median was used to reflect

the average carbon density and minimize the influence of outliers. The provincial-level vegetation and soil carbon density

160   data are listed in Table 2.

Table 2. Provincial vegetation and soil carbon density data

Province/region	Forest (Mg/ha)		Grassland (Mg/ha)	
	SOCD	VCD	SOCD	VCD
Chuan-Yu	98.83	55.96	143.09	1.25
Inner Mongolia	69.38	41.60	88.79	5.77
Liaoning	91.13	44.74	77.71	3.32
Jilin	95.09	73.85	67.09	3.06
Heilongjiang	145.45	64.63	93.58	2.98
Gan-Ning	99.44	36.80	54.66	3.80
Qinghai	75.87	30.54	108.60	6.45
Xinjiang	64.32	25.59	93.97	4.09
Xizang	129.33	82.43	58.89	4.20
Shanxi	59.98	40.63	56.13	8.77
Shaanxi	74.29	29.78	64.75	4.03
Shandong	60.42	42.29	/	/
Henan	59.03	42.41	/	/
Anhui	86.90	63.06	/	/
Hu-Ning	91.79	37.63	/	/
Hunan	92.60	51.94	/	/
Hubei	139.57	48.00	/	/
Jiangxi	93.29	50.81	/	/
Zhejiang	115.13	54.14	/	/
Fujian	117.71	58.80	/	/
Yue-Qiong	111.36	37.33	/	/
Guangxi	108.26	55.87	99.32	/
Yunnan	105.84	76.26	100.52	/
Guizhou	129.37	50.31	284.18	/

SOCD refers to soil organic carbon density, VCD refers to vegetation carbon density.

165

2.3 Methods

Annual emissions of carbon from land-use change were calculated with a bookkeeping model based on two types of data: rates of land-use change and per hectare effects of land-use change on carbon stocks. The former was calculated by constructing land-use transition rules, while the latter was derived from the disturbance response curves in the bookkeeping

170 model, combined with provincial vegetation and soil carbon density datasets.

2.3.1 Bookkeeping method

The method of bookkeeping was employed to estimate the annual carbon emissions caused by land-use changes in China from 1000 to 2019. Bookkeeping is widely used for estimating carbon emissions across multiple spatial and temporal scales. This method aimed to characterize the impacts of human-induced land-use changes on carbon stocks in vegetation and soil

175 across various terrestrial ecosystems (Qin et al., 2024; Yang et al., 2023; Bastos et al., 2021; Hartung et al., 2021). The

bookkeeping model used in this study is primarily driven by land-use change data and utilizes observed vegetation and soil carbon density data and specific disturbance response curves for each land-use transition type. As this method excludes the influence of unchanged land-use types and environmental changes, such as carbon dioxide concentrations and climate change, it quantifies direct anthropogenic fluxes and ignored carbon fluxes driven by environmental changes (Dorgeist et al., 2024; Houghton and Castanho, 2023). Consequently, the results of this method are frequently incorporated into global carbon budget estimates (Friedlingstein et al., 2023).

Our bookkeeping model uses statistical data rather than spatial grid data as input and calculates the net carbon change in terrestrial ecosystems due to land-use changes on an annual basis. The disturbance response curves specify the dynamic changes in carbon pools following land use transition, including biomass (both aboveground and belowground), litter (branches, trunks, roots, etc.), and soil organic carbon pools over time for each land-use type and per hectare of land-use change until a new carbon density equilibrium is reached (Houghton and Castanho, 2023). The response time for carbon release or absorption due to land-use changes can range from decades to centuries. Therefore, the carbon emission flux estimated at any given time includes both instantaneous and legacy fluxes from previous land-use changes. The calculation formula is as follows:

$$\Delta C_{flux}(j, t) = \sum_{k} \left(R_{LU}(j, k, t) \times C_v(j) \times f_{vge} \right) + \left(R_{LU}(j, k, t) \times C_s(j) \times f_{soil} \right) + \left(R_{LU}(j, k, t) \times C_v(j) \times f_{slash} \right) \qquad (3)$$

where $\Delta C_{flux}(j, t)$ is the carbon emission flux due to land-use change in province j at time t, $R_{LU}(j, k, t)$ is the land-use transition amount for type k in province j at time t, $C_V(j)$ and $C_s(j)$ are the vegetation and soil carbon densities in province j, respectively, and f is the disturbance response curve for vegetation and soil carbon pools. The values of f were derived from Houghton and Castanho (2023), see Appendix Table B2.

2.3.2 Reliability assessment of long-term land-use change data

Unlike modern geographic elements, which can be verified through techniques such as sample collection, field surveys, and remote sensing monitoring, historical land-use change data spanning long periods and large regions are difficult to independently validate because of temporal and spatial constraints. The reliability of such data is typically assessed through the examination of data sources, the rationality of the estimation or reconstruction methods, and the degree to which the results align with expert knowledge. Historical land-use data for China from global datasets were known to have poor support of local expert and knowledge and thus failed to capture China's recent land use dynamics (Yu et al., 2022). For this reason, we utilized regionally reconstructed historical land-use change data for China. We argue that the latter provides a more reliable representation of land-use trajectories in China over the past millennium. Below we further detail the rationale behind this choice.

The historical cropland data used in this study are typical examples of regionally reconstructed data. Historically, China has been a major agricultural nation, with agriculture forming the primary pillar of socioeconomic development in ancient

Chinese society. Cropland area directly influences agricultural tax revenues, and as a result, tax records for cropland areas have been extensively documented in the historical literature, making them highly reliable. Furthermore, although these records may not precisely correspond to actual croplands, scholars have developed conversion mechanisms to correspond tax records with actual cropland area across different historical periods. These methodologies have been used to reconstruct

210 cropland areas over various periods (Yang et al., 2024; Li et al., 2020; Li et al., 2018a; Li et al., 2018b; Li et al., 2016; Ge et al., 2004). These results have been peer-reviewed and published to ensure the reliability of the data sources, methods, and processes. Although global historical land-use datasets (such as the HYDE 3.2 dataset) have partly incorporated these regional reconstructions to reflect historical cropland changes at the national level for China, they are prone to error at provincial scale. Detailed analyses and assessments of the provincial errors in the global datasets can be found in Zhao et al.

215 (2022) and Fang et al. (2020).

Historical records of the forests in China are mainly scattered in various historical texts. While it is challenging to achieve a quantitative reconstruction of forest cover change based solely on literary sources, qualitative descriptions can be successfully made and several key features of forest changes in China over time were revealed: (1) northern China has a long history of deforestation: as early as a thousand years ago, forests in the North China Plain were already nearly depleted; (2)

220 over the following millennium, deforestation gradually expanded from plains and hills to mountainous areas; and (3) the deforestation process started from around the middle and lower reaches of the Yellow River and gradually extended to the middle and lower reaches of the Yangtze River, and then to the southern coastal areas of China, Southwest China, and Northeast China. These features provide crucial evidence for assessing the reliability of reconstructed forest data. By constructing a non-linear "inverted S-shaped" relationship between forest cover change and population size data, historical

225 forest area changes used in this study were estimated based on qualitative records of deforestation in Chinese history (He et al., 2024). In contrast, global historical land-use datasets depict historical forests in China by subtracting the area of cropland and pasture from the potential forest vegetation area in each grid cell simulated by vegetation modeling. This approach hence primarily reflects the transition of forest cover to human land-use and fails to accurately capture other factors that influence forest area changes, such as fuelwood and timber consumption. For a detailed evaluation of historical forest data in global

230 datasets for China, please refer to Yang et al. (2020).

For historical changes in grassland area, global datasets such as HYDE, SAGE, and PJ are based on the FAO's definition of pasture. However, Chinese scholars use the plant geography definition of grassland. This conceptual difference is one of the major reasons for the large discrepancies in grassland area for China between global datasets and the reconstructions generated by Chinese scholars (He et al., 2018). Unlike Europe and North America, where climate-driven land-use patterns

235 for livestock (grassland) dominate, China, especially in the eastern regions, has historically developed a cropland-based husbandry system under a monsoon climate, with relatively smaller-scale grassland agriculture. Therefore, global datasets based on European and North American land-use practices, which use historical population and per capita pasture area as

proxies to derive pasture or grassland data, are not applicable to China. For an evaluation of historical grassland data for China in global datasets, refer to He et al. (2018). The historical grassland cover data used in this study (He et al., 2024) are

240 based on historical cropland and forest data. These historical data consider the occupation of grassland by cropland expansion in western and northern China and also reflect the dynamic relationship between deforested land and secondary grasslands in eastern and southern China.

Overall, the long-term land-use data used in this study were based on historically reconstructed data rather than retrospective simulation data, with independent reconstructions performed for historical cropland and forest data.

245 Consequently, these reconstructed data are closer to historical facts and provide unique value for assessing the environmental effects of long-term human land-use changes.

2.3.3 Calculating annual land-use change

The high-confidence, long-term land-use data compiled for China, specifically of cropland, forest, and grassland data, do not cover all land types. Therefore, this study refers to the land-use types used in the carbon emission estimation by Houghton

250 and Castanho (2023) and major land-use types listed in the FAO (2021) report. Following the approach outlined by Houghton and Castanho (2023), we classify land types other than these three as "other land", thus defining four land-use categories: cropland, forest, grassland, and other land. The first three land-use types were derived from reconstructed data and survey statistics, as shown in Fig. 2 and Table 1. The "other land" category refers to the residual area in a province after excluding cropland, forest, and grassland, and it encompasses all land types not covered by the three primary land-use

255 categories. Compared with contemporary land-use classification standards, our "other land" category includes a variety of both human-affected and unaffected land types.
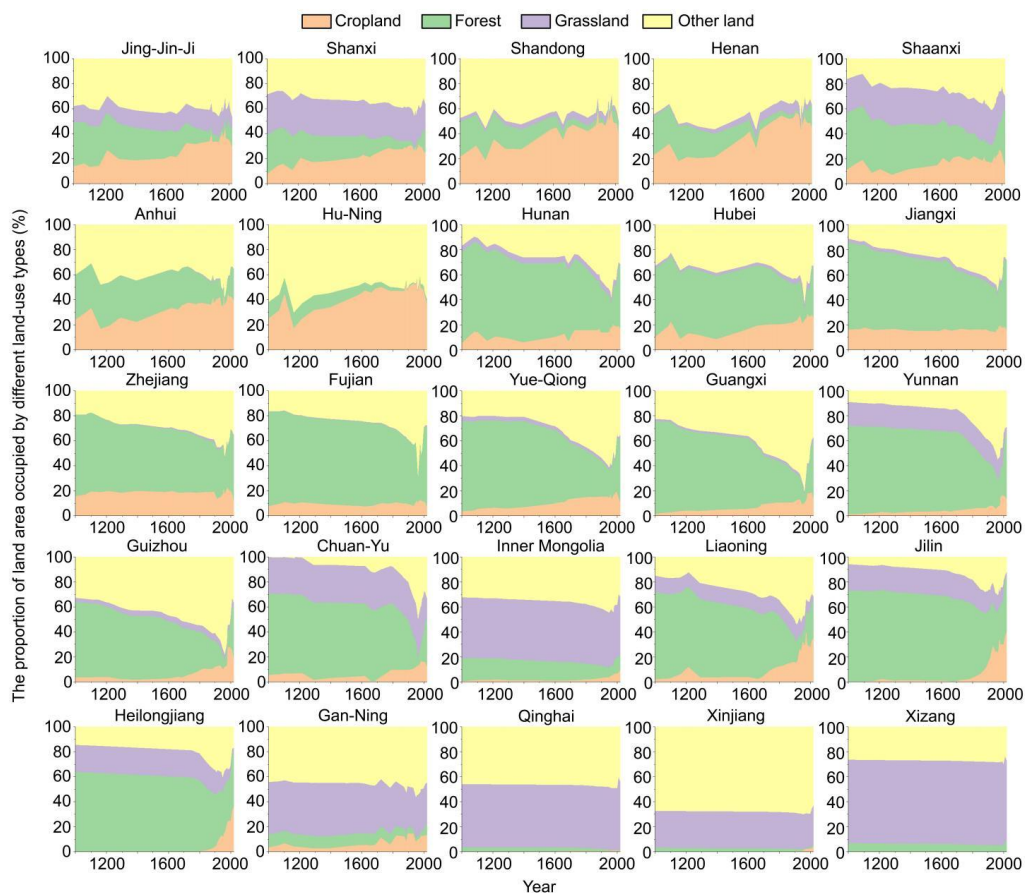
Figure 2. Percentage of the area of cropland, forest, grassland, and other land at the provincial scale.

260

Land-use products derived from remote sensing imagery are spatially explicit, thereby enabling the clear identification of land-use type transitions. However, the provincial-level reconstructed data used in this study lacked explicit spatial location information, and the conversion relationships between different land-use types were not always clear. Therefore, calculating annual land-use conversion rates is challenging. When only two land use types were involved and the increase (or decrease) in one land-use type exactly matches the decrease (or increase) in the other type, the conversion between land-use types is relatively straightforward. However, when more than two land-use types were involved in land use change, the conversion relationships become complex. To address this latter issue, we established rules to prioritize land-use conversions (Fig. 3).
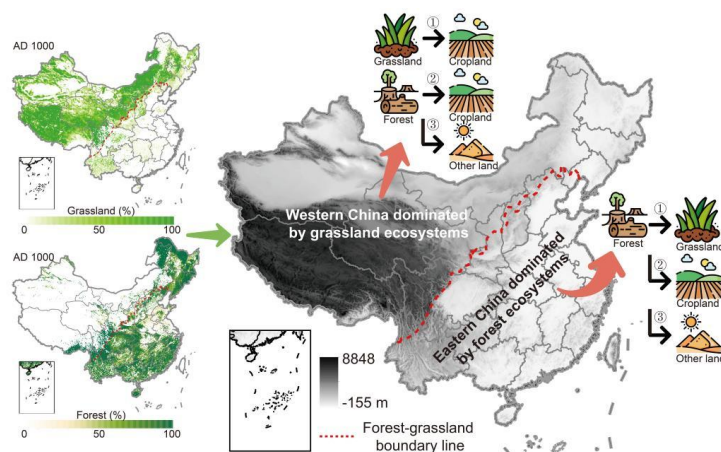
270   **Figure 3.** Historical land-use change transition rules. Numbers ①, ②, and ③ represent the priority levels.

From the land-use change data we employed, changes in grassland area and their conversion relationships were the most clearly defined. In western China, where grassland ecosystems dominate, changes in grassland areas primarily reflect the encroachment of croplands (He et al., 2024). Therefore, for western China, the conversion between grassland and cropland

275   was determined first based on changes in grassland area (Fig. 3). Second, the reduction in forest area was prioritized for conversion to cropland, followed by conversion to other land. In eastern China, where forest ecosystems are predominant, historical grasslands mainly consist of secondary grasslands resulting from the secondary succession of deforested lands (He et al., 2024). Hence, in eastern provinces dominated by forest ecosystems, the conversion between grassland and forest can be similarly determined based on changes in the grassland area. The remaining forest area was then prioritized for

280   conversion to cropland, followed by conversion to other land. Based on these rules, we calculated the annual land-use change rates in China from 1000 to 2019.

Houghton and Castanho (2023) proposed four alternative explanations for forest conversion to other land. Explanation 1: Forest loss is overestimated. Explanation 2: Forests are converted to shifting cultivation. Explanation 3: Forests are converted to new cropland, while an equal area of cropland is abandoned and undergoes degradation. Explanation 4: Forests

285   are converted to new cropland, and an equal area of cropland is abandoned, and subsequently restored to forest over a long period. Historically, shift cultivation (through deforestation) was common. Shift cultivation is a primitive and underdeveloped agricultural practice in which farmers clear land by burning and cultivating it extensively to obtain agricultural products. Once the soil fertility is exhausted, the farmers abandon cultivation and continue to clear new land. This practice has been widespread historically and continues today in the tropical rainforest regions of South America, Africa,

290   and Southeast Asia (Heinimann et al., 2017). Based on the characteristics of forest cover change documented in the Chinese historical literature, attributing forest loss, other than conversion to cropland and grassland, to shift cultivation aligns more

closely with historical facts. This form of agriculture has been recorded extensively in Chinese historical documents.

From the annual changes in cropland, forest, and grassland areas over the past millennium (Fig. 4a), it is evident that between the 18th and mid-20th centuries, the annual loss of forest area greatly exceeded the annual increase in cropland area.

295   Based on the conversion rules assumed here, we derived the annual change in other land (primarily shift cultivation) over the past millennium (Fig. 4b). The data revealed that shift cultivation was prevalent throughout history, although its scale was relatively small before the 18th century, with an average annual increase of 6.22×10^4 ha. However, after explosive population growth occurred in China, people under the pressure of survival expanded to hilly and mountainous forestlands, converting large areas of forest into shift cultivation. The average annual increase in shifting cultivation during this period reached 40.54

300    $\times 10^4$ ha, which was 6.5 times that of the previous period.
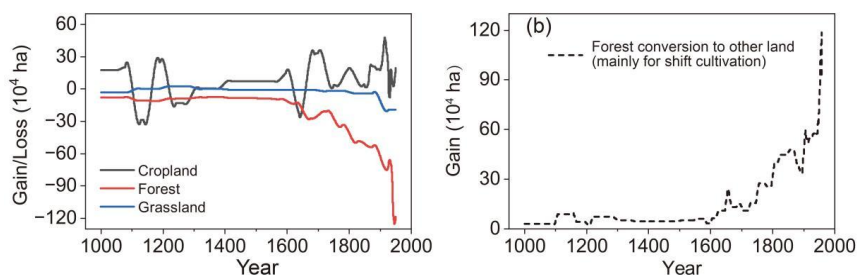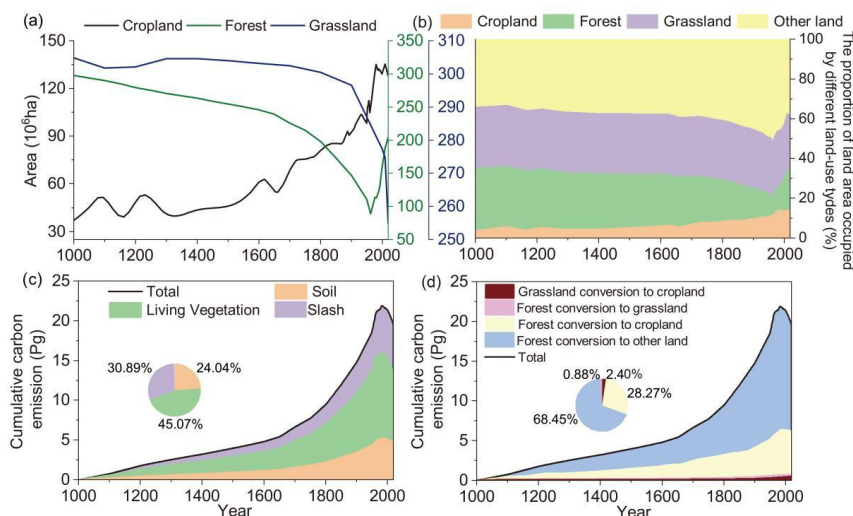

Figure 4. Changes in cropland, forest, grassland, and other land areas.

3. Results

305   **3.1 Overall carbon emissions**

Fig. 5 illustrates the land-use changes and associated carbon emissions in China over the past millennium. From 1000 to 2019, cumulative carbon emissions resulting from land-use changes totaled 19.61 Pg C, with the highest cumulative emissions occurring around 1980, reaching 21.87 Pg C. Overall, due to lag effects, the carbon emission trajectory did not fully align with the timeline of land-use changes. Specifically, the reversal of forest area decline (i.e., the transition from

310   forest loss to forest regrowth) occurred in the 1960s (Figs. 5a and 5b), whereas the reversal of the carbon budget from carbon source to carbon sink occurred in the 1980s. Approximately 30% of the annual carbon emission flux was attributable to residual emissions from historical periods.
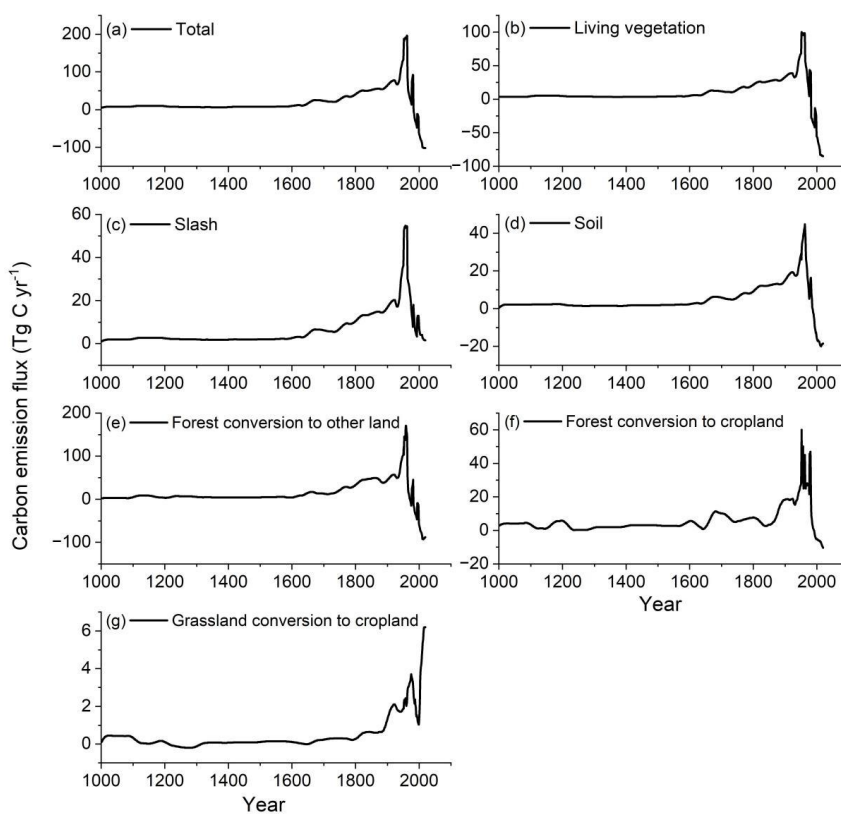
Figure 5. Annual land-use changes and carbon emissions in China from 1000 to 2019. (a) Changes in cropland, forest, and grassland area. (b) Proportions of cropland, forest, grassland, and other land. (c) Cumulative carbon emissions from land-use changes across different carbon pools. (d) Cumulative carbon emissions from different land-use transitions.

Based on the clear temporal trajectories, four distinct phases of carbon emissions were identified. Phase 1 (1000–1700): A slow growth phase for carbon sources, driven by deforestation, cropland expansion, and grassland reclamation, which resulted in a cumulative carbon emission of 6.60 Pg C, accounting for 30.17% of the total carbon emissions. The average annual carbon emission in this phase was 9.46 Tg C yr^{-1} (Fig 6a). Phase 2 (1700–1980): A rapid growth phase for carbon sources during which croplands expanded significantly beyond traditional agricultural areas in China, moving to southwest, northeast, and northwest China, accompanied by large-scale deforestation and grassland reclamation. Cumulative carbon emissions during this period reached 15.27 Pg C, accounting for 69.86% of the total emissions. The average annual loss was 54.09 Tg C yr^{-1}, 5.7 times that of Phase 1. Phase 3 (1980–1998): A phase dominated by large-scale afforestation, the carbon budget for land-use changes shifted from being a carbon source to a carbon sink. Between 1980 and 1998, carbon sink amounted to 0.12 Pg C, with an average annual carbon sink of 16.85 Tg C yr^{-1}. Phase 4 (1998–2019): An enhanced carbon sink phase attributed to the widespread implementation of large-scale forestry projects. During this period, the total carbon sink reached 1.85 Pg C (Figs. 5c and 5d), with an average annual carbon sink intensity of 88.21 Tg C yr^{-1} (Fig 6a), which was 5.2 times higher than that of Phase 3.

Regarding carbon pool types, the vegetation carbon pool stood out as the largest contributor of total emissions, accounting for 45.07% of the overall emissions (Fig. 5c). This was reflected in an average annual emission intensity of 8.67 Tg C yr^{-1} (Fig. 6b). Following closely was the slash carbon pool, which contributed 30.89%, with an average annual emission intensity of 5.95 Tg C yr^{-1} (Fig. 6c). The soil carbon pool, while still significant, represented a smaller portion at 24.04%, emitting an average of 4.63 Tg C yr^{-1} (Fig. 6d). When considering the impact of land-use changes, the conversion of forest to other land

14

types, particularly shift cultivation, emerged as the most dominant factor. This conversion alone was responsible for a

staggering 68.45% of the total carbon emissions (Fig. 5d), with an average annual emission of 13.17 Tg C yr⁻¹ (Fig. 6e). The

conversion of forest to cropland followed, contributing 28.27% of the emissions, or 5.44 Tg C yr⁻¹ (Fig. 6f). In comparison,

340   the conversion of grassland to cropland had a relatively minor effect, accounting for just 2.40% of the emissions, equivalent

to 0.46 Tg C yr⁻¹ (Fig. 6g). Finally, the conversion of forest to secondary grassland had an almost negligible impact,

representing only 0.88% of total emissions, with an annual release of less than 0.01 Tg C yr⁻¹.


345   **Figure 6.** Annual carbon emission flux of land-use changes in China from 1000 to 2019: total, carbon pools of soil, vegetation, and slash
and different land-use conversions. Annual carbon emission flux from forest conversion to grassland is less than 0.01 Tg yr⁻¹ and thus is
not presented in graphical form.

3.2 Regional carbon emissions

350   To facilitate the analysis of the spatiotemporal evolution of land-use carbon emissions, this study divided China into five

major regions: North China, Southeast China, Southwest China, Northeast China, and Northwest China (Fig. 7). North China

primarily refers to the North China Plain (Beijing, Tianjin, Hebei, Henan, Shandong, Anhui, and Jiangsu) and the provinces

Shanxi and Shaanxi. Southeast China includes the provinces Hubei, Hunan, Jiangxi, Zhejiang, Fujian, Guangdong, Hainan, and Guangxi. Southwest China consists of the provinces Sichuan, Chongqing, Guizhou, and Yunnan. Considering the forest

355   coverage in southeastern Xizang, this region is also categorized as part of Southwest China. Northeast China includes the provinces Liaoning, Jilin, and Heilongjiang as well as Inner Mongolia, where forest resources are mainly distributed in the Greater Khingan Range. Northwest China includes the provinces Gansu, Ningxia, Qinghai, and Xinjiang.
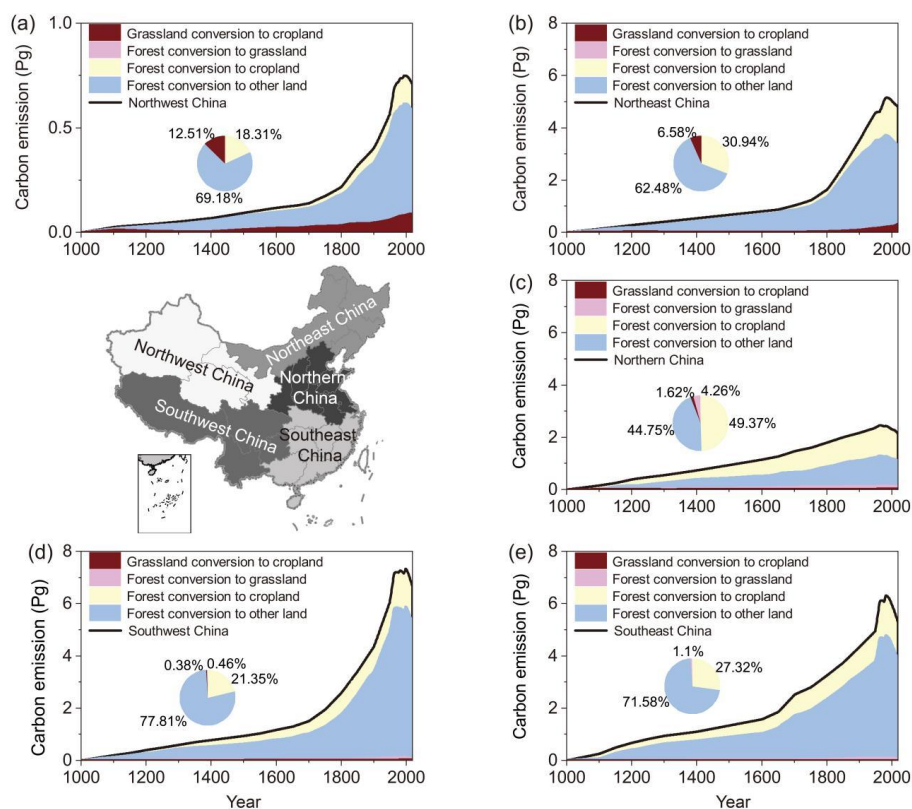
360   **Figure 7.** Cumulative carbon emissions and their proportions of land-use changes in different regions of China from 1000 to 2019.

Over the past millennium, Southwest China has recorded the highest cumulative carbon emissions, totaling 6.66 Pg C, followed by Southeast China with 5.29 Pg C and Northeast China with 4.81 Pg C. In contrast, North China accounted for 2.15 Pg C, and Northwest China recorded only 0.71 Pg C. Carbon emissions from land-use conversion in these regions showed significant variation. Notably, North China was distinct from the other regions, with the highest proportion of carbon

365   emissions resulting from the conversion of forests to croplands, accounting for 49.37% of the total (Fig. 7c). In the other four regions, the conversion of forests to other land types (mainly shift cultivation) contributed to the highest proportion of carbon emissions, with values of 71.58%, 77.81%, 62.48%, and 69.18%, respectively. The conversion of forests to secondary

grasslands occurred mainly in North China and Southeast China, contributing 4.26% and 1.1% of total carbon emissions,

370 respectively (Figs. 7c and 7e). The conversion of grasslands to cropland occurred mainly in Northwest and Northeast China,

accounting for 12.51% and 6.58%, respectively (Figs. 7a and 7b).

At the provincial scale, the years in which land-use changes shifted from carbon sources to carbon sinks varied across

regions (Appendix Fig. C1). During the carbon source period, seven provinces had cumulative carbon emissions exceeding

1.00 Pg C or an average carbon emission flux greater than 1.00 Tg C yr^{-1}, namely Chuan-Yu, Yunnan, Heilongjiang, Guangxi,

375 Inner Mongolia, Jilin, and Hunan. Among these, Chuan-Yu had the highest carbon emissions, reaching 3.28 Pg C (with an

average carbon emission flux of 3.35 Tg C yr^{-1}) (Fig. 8). The cumulative carbon emissions in eight provinces, including

Guizhou, Yue-Qiong, Liaoning, Hubei, Fujian, Jiangxi, Xizang, and Jing-Jin-Ji, ranged between 0.55 and 0.97 Pg C (average

carbon emission flux of 0.58–0.99 Tg C yr^{-1}). The remaining 10 provinces had cumulative carbon emissions of less than 0.50

Pg C, with Hu-Ning having the lowest at 0.11 Pg C (0.11 Tg C yr^{-1}). During the carbon sink period, the contribution of

380 carbon sequestration by each province followed a ranking similar to that of its carbon emissions during the carbon source

period. The Chuan-Yu region contributed 0.39 Pg C to the carbon sink, with a flux of 10.35 Tg C yr^{-1}. This indicates that

provinces with significant carbon emissions owing to widespread deforestation and agricultural expansion in historical

periods have played an important role as carbon sinks in recent decades, largely through large-scale afforestation and other
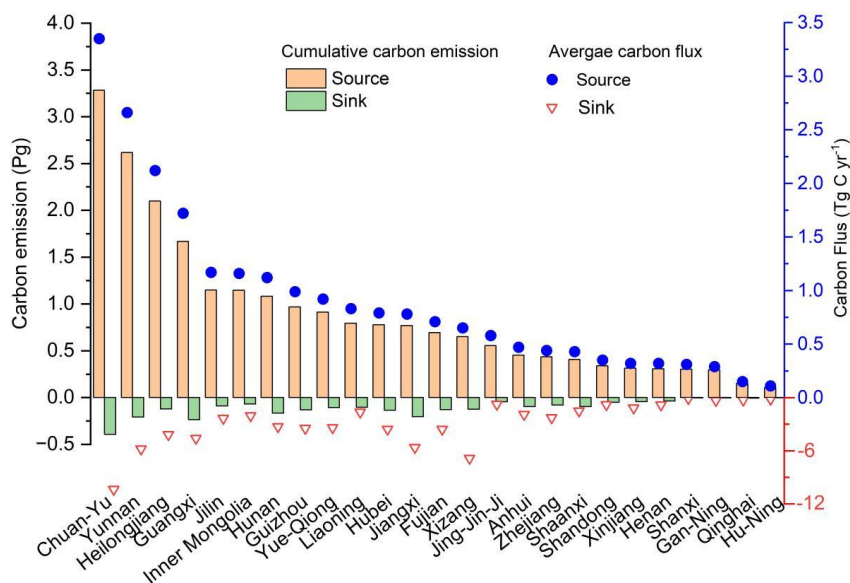
interventional measures.

385

Figure 8. Cumulative carbon emissions and average carbon flux at the provincial scale from 1000 to 2019.

4. Discussion

4.1 Review of estimation methods

390   Compared with the carbon emission estimates from land-use changes in China over the past 300 years by Yang et al. (2023), this study updated and improved the land-use change data, carbon density data, and disturbance response curves. The specific improvements were as follows. (1) Building on multiple recent studies, the land-use change data for China from 1700 to 1980 were extended back to AD 1000 and up to 2019, resulting in a land-use dataset with 131 time points spanning from 1000 to 2019. (2) In the calculation of land-use change rates, Yang et al. (2023) adjusted cropland data to align with 50-

395   and 100-year time intervals, matching those of the forest and grassland data. However, cropland data from historical periods, which were reconstructed based on tax records for cropland areas in historical archives, are highly accurate and record rich information on cropland coverage changes. Adjusting to 50- and 100-year intervals often obscures many signals of cropland cover change, whereas this study preserved all such information. (3) In the process of collecting carbon density data, we incorporated the results from China's Soil Survey Series, specifically the "Soil Series Atlas of China," which compiled 1,253

400   soil carbon density samples for various land cover types, including forests and grasslands. This significantly enriched the carbon density sample database, making the data more representative. (4) In the calculation of provincial carbon density, we assessed the normal distribution characteristics of the carbon density sample data for each province and chose either the arithmetic mean or median to obtain provincial average carbon densities, minimizing the influence of abnormally high or low values in the samples. (5) When calculating land-use change rates, although Yang et al. (2023) acknowledged that forest

405   conversion to cropland was far greater than cropland expansion, the classification of excess forest loss was not clearly explained. This study, which was based on the global historical land-use change scenarios of Houghton and Castanho (2023) and extensive historical records of deforestation in China, classified the remaining forest change, excluding cropland occupation, as shift cultivation, which is more aligned with historical facts. Based on this, we developed land-use conversion rules suitable for provincial-level analysis in China and incorporated the methods and characteristics of cropland, forest, and

410   grassland dataset reconstruction. (6) The disturbance response curve was central to the bookkeeping model, driving the calculation of carbon budgets using annual land-use change rates and carbon density data. In this study, we used an improved disturbance response curve (Houghton and Castanho, 2023). In summary, this study updated and improved both the data and models covering six specific areas, thereby increasing the reliability of carbon emission estimates.

4.2 Comparison with previous estimates

415   Many scholars have achieved progress in estimating carbon emissions based on long-term land-use changes in China. Among them, Houghton and Castanho (2023), Yang et al. (2023), Yang et al. (2019), Li et al. (2014), and Ge et al. (2008) are particularly comparable to this study because of their long time spans, broad scope, and use of bookkeeping models. Although these studies covered different periods, they are generally comparable within the context of the past 300 years,

which is not entirely accurate.

420   Using the annual carbon flux estimates in this study, we calculated carbon emissions over periods comparable to those of related studies (Table 3). Specifically, the cumulative carbon emissions from 1700 to 1980 in this study were 68% higher than those estimated by Yang et al. (2023) (Table 3). This difference was primarily due to the significant reduction in forest area, which far exceeds the expansion of cropland in historical periods. This study clearly identified the source of this change as shift cultivation. The carbon emissions from 1661 to 1980 in this study were 4.28 times higher than those reported by

425   Yang et al. (2019), mainly because the latter only considered the expansion of cropland and the conversion of forest and grassland. From 1700 to 1949, the carbon emissions in this study were 92% higher than those reported by Ge et al. (2008), which was mainly because of differences in the land-use change rate calculation rules and underlying vegetation and soil carbon density data. At the regional scale, the carbon emissions in this study from 1680 to 1980 in Northeast China (Heilongjiang, Jilin, and Liaoning) were 130% higher than those estimated by Li et al. (2014). Furthermore, this study used

430   an improved bookkeeping model, whereas Yang et al. (2019), Li et al. (2014), Ge et al. (2008), and Yang et al. (2023) all relied on an earlier version, which is another significant source of difference. Overall, the carbon emission estimates in this study were 68% to 328% higher than those of previous studies, indicating that previous estimates of carbon emissions from land-use changes in China have been severely underestimated.

435   **Table 3.** Comparison of existing long-term carbon emission estimation results caused by land-use change in China

Region	Method	Time period	Previous study (Pg C)	Reference	This study (Pg C)
China	Bookkeeping model (Early version)	1700–1980	9.05	Yang et al. (2023)	15.17
China	Bookkeeping model (Early version)	1661–1980	3.78	Yang et al. (2019)	16.13
China	Bookkeeping model (Early version)	1700–1949	6.18	Ge et al. (2008)	11.87
Northeast China (Heilongjiang, Jilin, and Liaoning)	Bookkeeping model (Early version)	1680–1980	1.45	Li et al. (2014)	3.33
Global	Bookkeeping model (Latest version)	1850–2019	7.36	Houghton and Castanho (2023)	7.72
China	Land ecosystem model	1900–1980	6.90	Yu et al. (2022)	7.07
China	Land ecosystem model	1980–2019	8.90	Yu et al. (2022)	2.25

At the national level, there is considerable uncertainty among the different methods used to estimate carbon emissions from land-use changes in China. From the carbon emission flux change curve, the estimates in this study fall within the range of existing model estimates at an intermediate level (Fig. 9). Specifically, the cumulative emissions estimated in this

440   study are close to those of Houghton and Nassikas (2017), particularly those of Houghton and Castanho (2023) for China

(Table 2), partly because all three rely on the same bookkeeping model. Nevertheless, there were significant differences in the carbon flux peaks and valleys among the three studies (Fig. 9), mainly because of substantial differences in the provincial-level land-use data. The other three bookkeeping model estimates aligned more closely with the trends in the DGVM$_S$ estimates, which were driven by the global long-term global land-use dataset (LUH2), with differences in numerical

445   values mainly arising from differences in model parameters (Obermeier et al., 2024; Friedlingstein et al., 2019; Hansis et al., 2015). These models significantly overestimated the carbon emission flux from land-use changes compared with the results of this study.
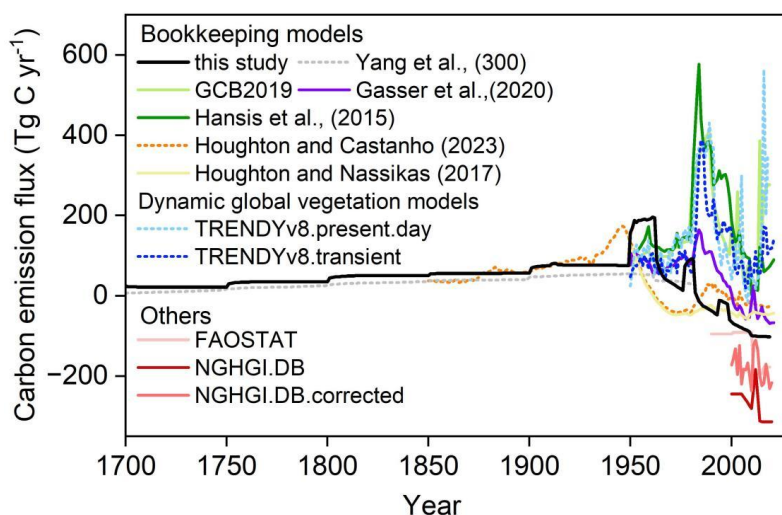
450   **Figure 9.** Chinese historical land-use change-induced carbon emission flux estimated by different methods.

Additionally, the estimates from this study differed considerably from national report-based data (e.g., NGHGIs and FAOSTAT) (Fig. 9) (Obermeier et al., 2024), possibly because national reports specifically account for afforestation and ecological restoration projects with high carbon removal potential. The most direct example is the similarity between our

455   estimated carbon emissions (1900–1980) and the results of Yu et al. (2022) (Table 3) which was because of the lack of significant or widespread land management or engineering projects in China during this period. However, the estimates for 1980–2019 differed greatly because land management practices during this period had a substantial impact. As revealed by Yue et al. (2024), land management has played a crucial role in China's land-carbon balance since 1980.

4.3 Uncertainty analysis

460   The long-term land-use data used in this study, including reconstructed and derived data from statistical surveys, represent the net land-use values within the statistical units. However, actual land-use changes, as indicated by remote sensing data, show that within a given area of a particular land-use type, there are pixels where the area has increased and pixels where the

Earth System
Open Access
Science
Discussions
Data

area has decreased. The total change due to these increases and decreases is much greater than the net change, and such detailed variations cannot currently be captured by long-term historical land-use datasets. Therefore, uncertainty in basic

465   land-use data leads to inherent uncertainty in the estimated carbon budget associated with land-use changes.

When calculating annual land-use change rates, the classification of land-use types is relatively coarse due to data limitations. Land-use types other than cropland, forest, and grassland are all grouped together as "other land," and land-use conversion rules are established based on this classification to calculate the annual land-use change rates. Compared with modern remote sensing-based land-use data, long-term land-use data are less detailed, which also affects the accuracy of

470   carbon budget estimates related to land-use change.

Additionally, the spatiotemporal variability of basic carbon density values can influence the accuracy of the estimates. In this study, carbon density is addressed using a "present-day-for-past" substitution method. Although modern soil carbon densities have been moderately adjusted by incorporating a large-scale soil sampling survey dataset from the post-1949 period in China, the inherent spatiotemporal variability of carbon density introduces additional uncertainty because when

475   static values are substituted for past periods, dynamic changes may not be fully captured.

5. Data availability

Annual carbon emissions from land-use change in China for 1000–2019 are available at https://doi.org/10.5281/zenodo.14557386 (Yang et al., 2025).

6. Conclusion

480   Reducing the uncertainty in carbon budget estimates from land-use change has become a frontier in global change science and is receiving widespread attention, as it plays a crucial role in achieving the global "carbon neutrality" target. This study provides an estimation of the annual carbon emissions from land-use changes in China from 1000 to 2019. High-confidence long-term land-use change datasets, extensive vegetation and soil carbon density sampling data, and newly developed disturbance response curves effectively minimized the uncertainties in previous long-term carbon budget estimates for

485   China.

From 1000 to 2019, carbon emissions resulting from land-use changes in China amounted to 19.61 Pg C. Four distinct phases were identified. The first phase, which occurred before the early 18th century (1000–1700), saw a slow increase in carbon sources, with a total emission of 6.60 Pg C, accounting for 30.17% of the total, at an average annual rate of 9.46 Tg C yr^{-1}. The second phase, which occurred from the early 18th century to the early 1980s (1700–1980), experienced rapid

490   growth in carbon sources (15.27 Pg C, 69.86%, 54.09 Tg C yr^{-1}). The third phase, which occurred from the 1980s to the late 1990s (1980–1998), saw a reversal in the carbon balance, with land-use changes shifting from carbon sources to carbon sinks

(carbon sink of 0.12 Pg C, 16.85 Tg C yr⁻¹). The fourth phase, which occurred from the late 1990s to 2019 (1998–2019), saw a further enhancement of the carbon sink (1.85 Pg C, 88.21 Tg C yr⁻¹).

495 **Author contributions.** FY and GD designed the work. FY, FH and ML provided historical provincial cropland, forest, and grassland data for quantifying China's annual carbon budget from land-use change. FY, WL, ZL, and XZ collected vegetation and soil carbon density sample points data. RAH provided the disturbance-response curve parameter table. FY, XM, RAH and YG devised the land-use transition rules. FY, GD, XM, HZ, PW, FH, QM, YY and CY reviewed and edited the text. FY prepared the manuscript and wrote the final paper with contributions from all coauthors.

500

Competing interests. One of the (co-)authors is a member of the editorial board of Earth System Science Data.

505

Appendix A

Table A1. Detailed reference for the second and third national land survey bulletins.

Items	Time point	Land-use types	Province	Data source/Download link
The Second National Land Survey of China	2009	cropland, forest, and grassland	all provinces	https://gtdc.mnr.gov.cn/shareportal#/
			Henan	https://www.henan.gov.cn/2022/04-18/2433857.html
			Shanxi	http://www.shanxi.gov.cn/ywdt/zwlb/bmkx/202201/t20220127_6441197.shtml
			Shandong	http://dnr.shandong.gov.cn/zwgk_324/xxgkml/ywdt/tzgg_29303/202112/t20211216_3810111.html
			Hebei	https://zrzy.hebei.gov.cn/heb/gongk/gkml/gggs/qtgg/zrdcc/10671417206794772480.html
			Liaoning	https://www.ln.gov.cn/web/ywdt/jrln/wzxx2018/EFA7CA9476D44D8D85578D867D70EA56/index.shtml
			Jilin	http://www.jl.gov.cn/szfzt/xwfb/xwfbh/xwfbh2021/jlsdssjrmdbdhdychy_409635/
			Heilongjiang	http://www.dview.com.cn/rjcp_zz_3741.html
			Jiangsu	http://news.yznews.com.cn/2021-12-31/content_7347606.htm
			Zhejiang	https://zrzyt.zj.gov.cn/art/2021/12/3/art_1289933_58988406.html
			Anhui	https://zrzyt.ah.gov.cn/public/7021/146407571.html
The Third National Land Survey of China	2019	cropland, forest, and grassland	Fujian	http://zrzyt.fujian.gov.cn/zwgk/zfxxgkzl/zfxxgkml/tdgl_19753/202112/t20211231_5805488.htm
			Jiangxi	http://bnr.jiangxi.gov.cn/art/2021/12/29/art_35804_3810534.html
			Hubei	https://zrzyt.hubei.gov.cn/fbjd/xxgkml/sjfb/tdzytjsj/202112/t20211217_3919353.shtml?eqid=e3b66db3004cc51a00000006647fe835
			Hunan	http://www.hunan.gov.cn/hnszf/zfsj/sjfb/202112/t20211207_21275973.html?share_token=83aa6011-7231-4c49-8a14-a14f9ae0c29b
			Guangdong	http://www.jiangmen.gov.cn/jmzrj/gkmlpt/content/2/2507/post_2507058.html?eqid=87430417001fc53900000003648a53ca#187
			Hainan	https://www.hainan.gov.cn/hainan/0101/202110/8c92db59ef6f4468b96b058465ba60b2.shtml
			Sichuan	http://dnr.sc.gov.cn/scdnr/scsdcsj/2022/1/18/3e1bc5eb55db44628498b5db740eac5b.shtml
			Guizhou	http://www.guizhou.gov.cn/zwgk/zdlygk/jjgzlfz/zrzy/zrzydcjcgl/202201/t20220121_72378280.html
			Yunnan	https://www.yn.gov.cn/sjfb/tjgb/202112/t20211221_231929.html

Shaanxi	https://zrzyt.shaanxi.gov.cn/info/1038/57862.htm?eqid=892a22b000028c4b00000006644b72c5
Gansu	https://baijiahao.baidu.com/s?id=1712097491056856575&wfr=spider&for=pc
Qinghai	https://zrzyt.qinghai.gov.cn/gk/sj/zrzygb/content_4922
Beijing	https://ghzrzyw.beijing.gov.cn/zhengwuxinxi/sjtj/tdbgdctj/202111/t20211105_2529986.html
Tianjin	https://ghhzrzy.tj.gov.cn/zwgk_143/tzgg/202111/t20211118_5712899.html
Shanghai	https://ghzyj.sh.gov.cn/zcfg-tdgl/20220107/b513d306e88b41bebc7b7b8a5b5cc56c.html
Chongqing	http://tjj.cq.gov.cn/zwgk_233/fdzdgknr/tjxx/sjzl_55471/tjgb_55472/202111/t20211125_10031239.html
Inner Mongolia	https://zrzy.nmg.gov.cn/zwgk/tztg/202205/t20220507_2051673.html
Guangxi	https://dnr.gxzf.gov.cn/zfxxgk/fdzdgknr/tjfx/zhtj/t16084757.shtml
Xizang	http://zrzyt.xizang.gov.cn/gk/gsgg/202112/t20211224_276279.html
Ningxia	https://www.nx.gov.cn/zwgk/tzgg/202112/t20211206_3205422_zzb.html
Xinjiang	http://zrzyt.xinjiang.gov.cn/xjgtzy/gzdt/202201/c7061f858692402da4f7b65e376cd2fb.shtml

∗ Last access: May 2024.

Open Access Earth System Science Data Discussions

Appendix B

Table B1. Detailed information for soil series in China

Title	Publisher	Year
Soil Series in China: Anhui	Science Press	2017
Soil Series in China: Beijing and Tianjin	Science Press	2016
Soil Series in China: Hebei	Science Press	2017
Soil Series in China: Shandong	Science Press	2019
Soil Series in China: Henan	Science Press	2019
Soil Series in China: Jiangsu	Science Press	2017
Soil Series in China: Shanghai	Science Press	2017
Soil Series in China: Hubei	Science Press	2017
Soil Series in China: Fujian	Science Press	2017
Soil Series in China: Zhejiang	Science Press	2017
Soil Series in China: Hainan	Science Press	2018
Soil Series in China: Heilongjiang	Science Press	2020
Soil Series in China: Jilin	Science Press	2019
Soil Series in China: Liaoning	Science Press	2020
Soil Series in China: Guangdong	Science Press	2017
Soil Series in China: Central and Western Volume: Shanxi	Science Press Longmen Press	2020
Soil Series in China: Central and Western Volume: Shaanxi	Science Press Longmen Press	2020
Soil Series in China: Central and Western Volume: Inner Mongolia	Science Press Longmen Press	2020
Soil Series in China: Central and Western Volume: Ningxia	Science Press Longmen Press	2020
Soil Series in China: Central and Western Volume: Qinghai	Science Press Longmen Press	2020
Soil Series in China: Central and Western Volume: Hunan	Science Press Longmen Press	2020
Soil Series in China: Central and Western Volume: Jiangxi	Science Press Longmen Press	2020
Soil Series in China: Central and Western Volume: Sichuan	Science Press Longmen Press	2020
Soil Series in China: Central and Western Volume: Chongqing	Science Press Longmen Press	2020
Soil Series in China: Central and Western Volume: Gansu	Science Press Longmen Press	2020
Soil Series in China: Central and Western Volume: Guangxi	Science Press Longmen Press	2020
Soil Series in China: Central and Western Volume: Guizhou	Science Press Longmen Press	2020
Soil Series in China: Central and Western Volume: Yunnan	Science Press Longmen Press	2020
Soil Series in China: Central and Western Volume: Xinjiang	Science Press Longmen Press	2020

Soil Series in China: Central and Western Volume: Xizang	Science Press	2020
	Longmen Press	

Table B2. Disturbance response curve parameter.

Ecological zone	Land-use change	Soil decay	Soil recovery
Temperate Desert	FC, FO, GC	3% per year (first 4 years)	0.3% per year (50 years)
		1% per year (last 11 years)	
Temperate Steppe	FC, FO, GC	3% per year (first 4 years)	0.41% per year (37 years)
		1% per year (last 11 years)	
Temperate Continental	FC, FO, GC	3% per year (first 4 years)	0.3125% per year (48years)
		1% per year (last 11 years)	
Subtropical Humid	FC, FO, GC	3% per year (first 4 years)	0.3125% per year (48years)
		1% per year (last 11 years)	

Ecological zone	Land-use change	Living vegetation decay	Living vegetation recovery
Temperate Desert	FC, FO	95% per year (1 year)	0.02% per year (50 years)
			0.06% per year (30 years)
	FP	95% per year (1 year)	0.05% per year (28 years)
			0.09% per year (20 years)
Temperate Steppe	FC, FO	95% per year (1 year)	0.24% per year (37 years)
			0.09% per year (50 years)
	FP	90% per year (1 year)	0.11% per year (37 years)
			0.09% per year (50 years)
Temperate Continental	FC, FO	95% per year (1 year)	1.63% per year (48 years)
			0.56% per year (50 years)
	FP	90% per year (1 year)	1.99% per year (37 years)
			0.56% per year (50 years)
Subtropical Humid	FC, FO	95% per year (1 year)	1.63% per year (48 years)
			0.56% per year (50 years)
	FP	90% per year (1 year)	1.99% per year (37years)
			0.56% per year (50 years)

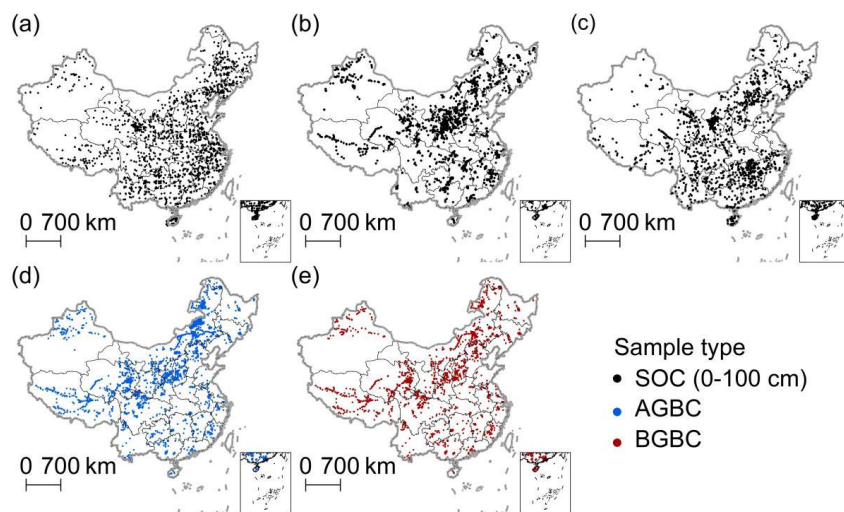| Ecological zone	Land-use change	Fraction Goes to Slash	Decay rate
Temperate Desert, Temperate Steppe, Temperate Continental	FC, FO	50%	10% each year based on the value of the previous year
	FP	33%	
Subtropical Humid	FC, FO	50%	50% each year based on the value of the previous year
	FP	33%	

Figure B1. Distribution of sample points for vegetation carbon density and soil carbon density. (a) SOC is derived from the 2010s China's terrestrial ecosystem carbon density dataset (Xu et al., 2019). (b) SOC is derived from the "Soil Chronicles of China." (c) SOC is derived from the "Soil Series of China." SOC refers to soil organic carbon. AGBC refers to above-ground biomass carbon, and BGBC refers to below-ground biomass carbon.
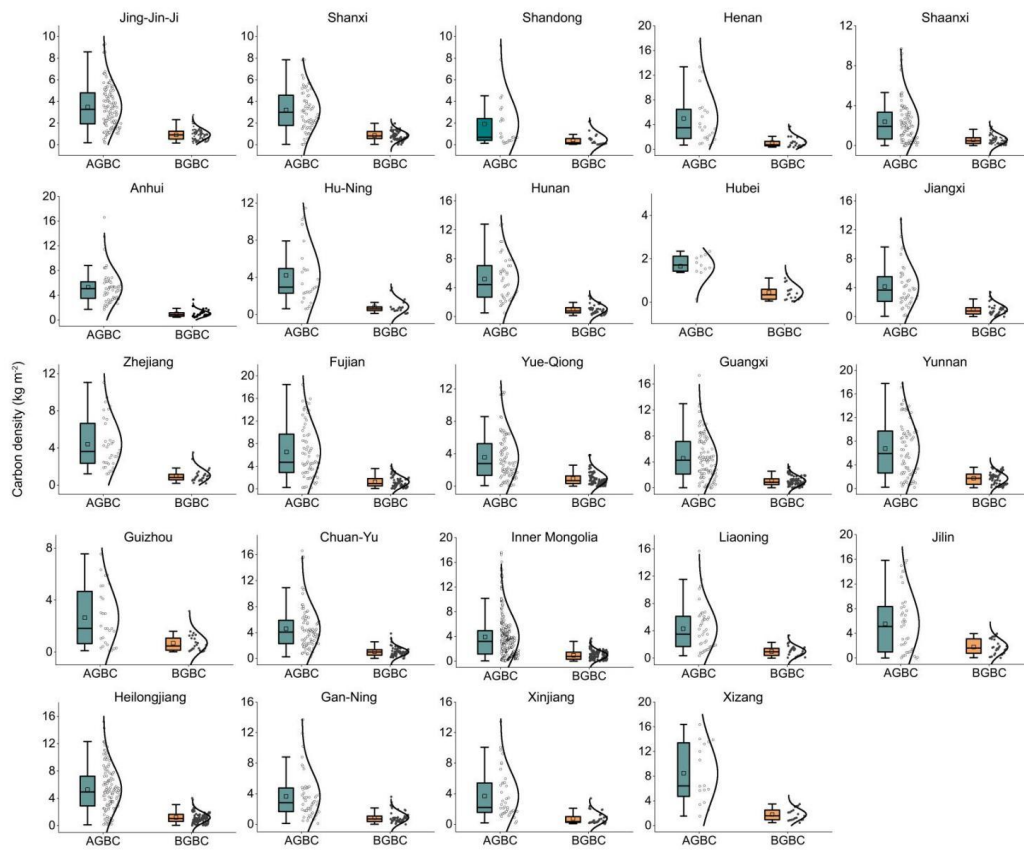
Figure B2. Distribution of forest vegetation carbon density at provincial scale. AGBC refers to above-ground biomass carbon, and BGBC refers to below-ground biomass carbon.
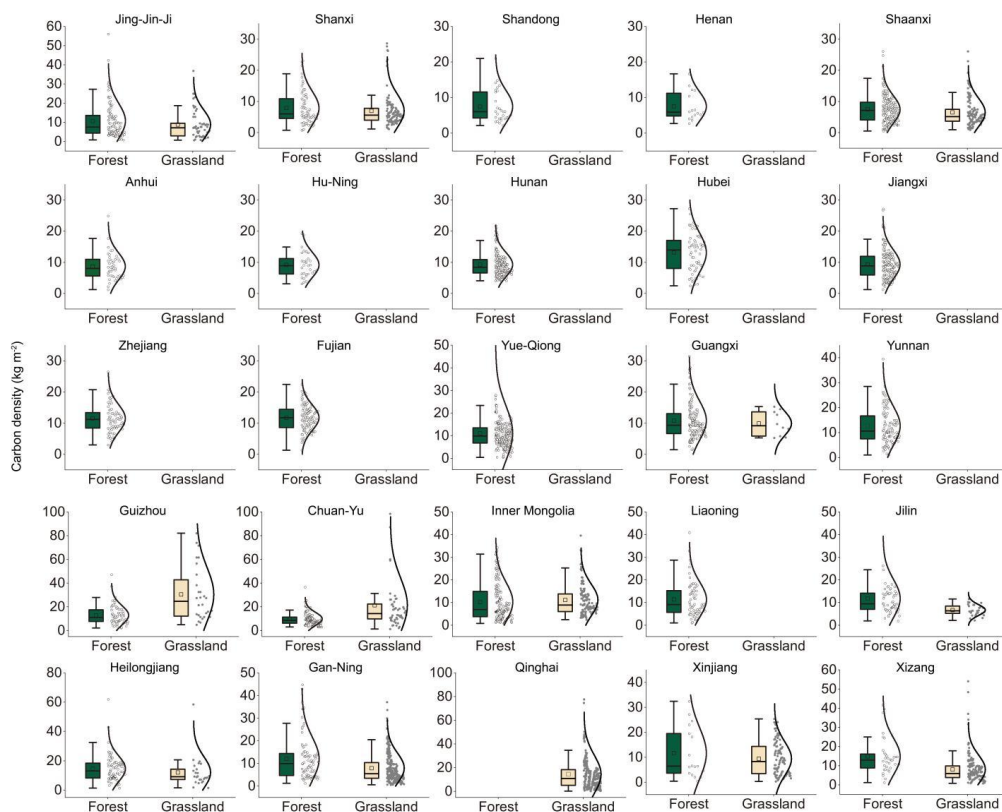
Figure B3. Distribution of soil carbon density in forests and grasslands at provincial scale.
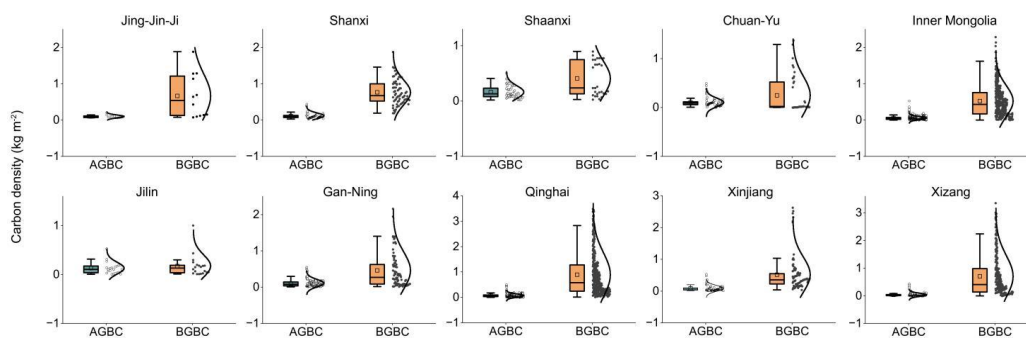

Figure B4. Distribution of grassland vegetation carbon density at provincial scale. AGBC refers to above-ground biomass carbon, and BGBC refers to below-ground biomass carbon.
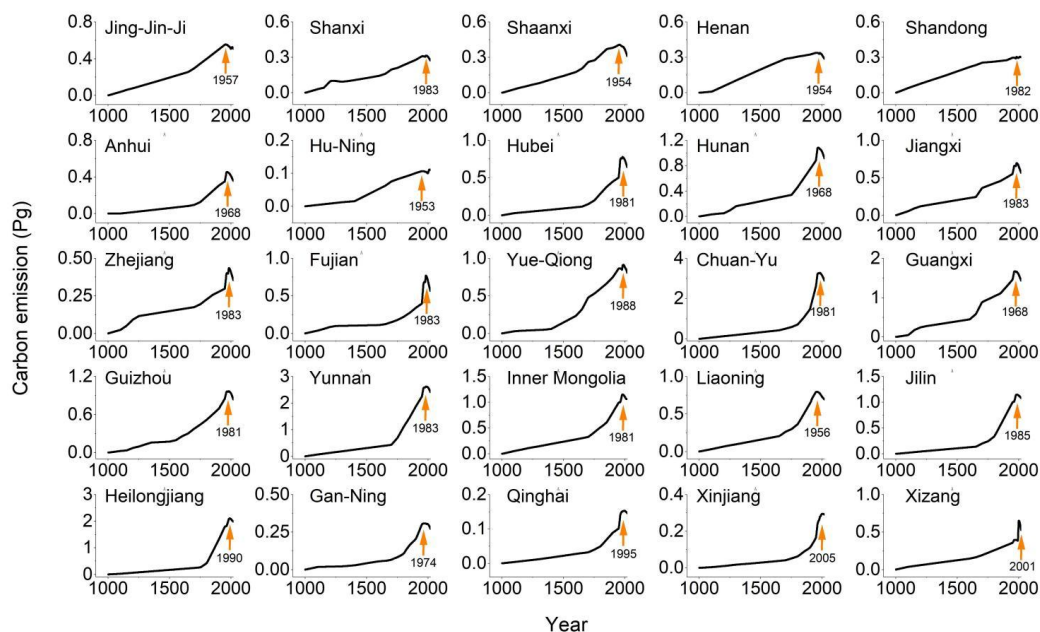
Appendix C

Figure C1. Cumulative carbon emissions from land-use changes at the provincial level. Arrows indicate the turning points from carbon sources to carbon sinks, with numbers representing the corresponding years of the turning points.

References

Bastos, A., Hartung, K., Nutzel, T. B., Nabel, J., Houghton, R. A., and Pongratz, J.: Comparison of uncertainties in land-use change fluxes from bookkeeping model parameterisation, Earth System Dynamics, 12, 745-762, 10.5194/esd-12-745-2021, 2021.

Dorgeist, L., Schwingshackl, C., Bultan, S., and Pongratz, J.: A consistent budgeting of terrestrial carbon fluxes, Nat Commun, 15, 7426, 10.1038/s41467-024-51126-x, 2024.

Fang, X. Q., Zhao, W. Y., Zhang, C. P., Zhang. D. Y., Wei, X. Q., Qiu W, Ye Y.: Methodology for credibility assessment of historical global LUCC datasets, Science China Earth Sciences, 63: 1013-1025, 10.1007/s11430-019-9555-3, 2020.

FAO: FAOSTAT Statistical Database, FAO, Rome, Extracted from: http://www.fao.org/faostat/en/#data/ (last access: October 2023), 2021.

Friedlingstein, P., Jones, M. W., O'Sullivan, M., Andrew, R. M., Hauck, J., Peters, G. P., Peters, W., Pongratz, J., Sitch, S., Le Quéré, C., Bakker, D. C. E., Canadell, J. G., Ciais, P., Jackson, R. B., Anthoni, P., Barbero, L., Bastos, A., Bastrikov, V., Becker, M., Bopp, L., Buitenhuis, E., Chandra, N., Chevallier, F., Chini, L. P., Currie, K. I., Feely, R. A., Gehlen, M., Gilfillan, D., Gkritzalis, T., Goll, D. S., Gruber, N., Gutekunst, S., Harris, I., Haverd, V., Houghton, R. A., Hurtt, G., Ilyina, T., Jain, A. K., Joetzjer, E., Kaplan, J. O., Kato, E., Klein Goldewijk, K., Korsbakken, J. I., Landschützer, P., Lauvset, S. K., Lefèvre, N., Lenton, A., Lienert, S., Lombardozzi, D., Marland, G., McGuire, P. C., Melton, J. R., Metzl, N., Munro, D. R., Nabel, J. E. M. S., Nakaoka, S.-I., Neill, C., Omar, A. M., Ono, T., Peregon, A., Pierrot, D., Poulter, B., Rehder, G., Resplandy, L., Robertson, E., Rödenbeck, C., Séférian, R., Schwinger, J., Smith, N., Tans, P. P., Tian, H., Tilbrook, B., Tubiello, F. N., van der Werf, G. R., Wiltshire, A. J., and Zaehle, S.: Global Carbon Budget 2019, Earth Syst. Sci. Data, 11, 1783–1838, https://doi.org/10.5194/essd-11- 1783-2019, 2019.

Friedlingstein, P., Jones, M. W., O'Sullivan, M., Andrew, R. M., Bakker, D. C. E., Hauck, J., Le Quéré, C., Peters, G. P.,

Peters, W., Pongratz, J., Sitch, S., Canadell, J. G., Ciais, P., Jackson, R. B., Alin, S. R., Anthoni, P., Bates, N. R., Becker, M., Bellouin, N., Bopp, L., Chau, T. T. T., Chevallier, F., Chini, L. P., Cronin, M., Currie, K. I., Decharme, B., Djeutchouang, L. M., Dou, X., Evans, W., Feely, R. A., Feng, L., Gasser, T., Gilfillan, D., Gkritzalis, T., Grassi, G., Gregor, L., Gruber, N., Gürses, Ö., Harris, I., Houghton, R. A., Hurtt, G. C., Iida, Y., Ilyina, T., Luijkx, I. T., Jain, A., Jones, S. D., Kato, E., Kennedy, D., Klein Goldewijk, K., Knauer, J., Korsbakken, J. I., Körtzinger, A., Landschützer, P., Lauvset, S. K., Lefèvre, N., Lienert, S., Liu, J., Marland, G., McGuire, P. C., Melton, J. R., Munro, D. R., Nabel, J. E. M. S., Nakaoka, S.-I., Niwa, Y., Ono, T., Pierrot, D., Poulter, B., Rehder, G., Resplandy, L., Robertson, E., Rödenbeck, C., Rosan, T. M., Schwinger, J., Schwingshackl, C., Séférian, R., Sutton, A. J., Sweeney, C., Tanhua, T., Tans, P. P., Tian, H., Tilbrook, B., Tubiello, F., van der Werf, G. R., Vuichard, N., Wada, C., Wanninkhof, R., Watson, A. J., Willis, D., Wiltshire, A. J., Yuan, W., Yue, C., Yue, X., Zaehle, S., and Zeng, J.: Global Carbon Budget 2021, Earth System Science Data, 14, 1917-2005, 10.5194/essd-14-1917-2022, 2022.

Friedlingstein, P., O'Sullivan, M., Jones, M. W., Andrew, R. M., Bakker, D. C. E., Hauck, J., Landschützer, P., Le Quéré, C., Luijkx, I. T., Peters, G. P., Peters, W., Pongratz, J., Schwingshackl, C., Sitch, S., Canadell, J. G., Ciais, P., Jackson, R. B., Alin, S. R., Anthoni, P., Barbero, L., Bates, N. R., Becker, M., Bellouin, N., Decharme, B., Bopp, L., Brasika, I. B. M., Cadule, P., Chamberlain, M. A., Chandra, N., Chau, T.-T.-T., Chevallier, F., Chini, L. P., Cronin, M., Dou, X., Enyo, K., Evans, W., Falk, S., Feely, R. A., Feng, L., Ford, D. J., Gasser, T., Ghattas, J., Gkritzalis, T., Grassi, G., Gregor, L., Gruber, N., Gürses, Ö., Harris, I., Hefner, M., Heinke, J., Houghton, R. A., Hurtt, G. C., Iida, Y., Ilyina, T., Jacobson, A. R., Jain, A., Jarníková, T., Jersild, A., Jiang, F., Jin, Z., Joos, F., Kato, E., Keeling, R. F., Kennedy, D., Klein Goldewijk, K., Knauer, J., Korsbakken, J. I., Körtzinger, A., Lan, X., Lefèvre, N., Li, H., Liu, J., Liu, Z., Ma, L., Marland, G., Mayot, N., McGuire, P. C., McKinley, G. A., Meyer, G., Morgan, E. J., Munro, D. R., Nakaoka, S.-I., Niwa, Y., O'Brien, K. M., Olsen, A., Omar, A. M., Ono, T., Paulsen, M., Pierrot, D., Pocock, K., Poulter, B., Powis, C. M., Rehder, G., Resplandy, L., Robertson, E., Rödenbeck, C., Rosan, T. M., Schwinger, J., Séférian, R., Smallman, T. L., Smith, S. M., Sospedra-Alfonso, R., Sun, Q., Sutton, A. J., Sweeney, C., Takao, S., Tans, P. P., Tian, H., Tilbrook, B., Tsujino, H., Tubiello, F., van der Werf, G. R., van Ooijen, E., Wanninkhof, R., Watanabe, M., Wimart-Rousseau, C., Yang, D., Yang, X., Yuan, W., Yue, X., Zaehle, S., Zeng, J., and Zheng, B.: Global Carbon Budget 2023, Earth System Science Data, 15, 5301-5369, 10.5194/essd-15-5301-2023, 2023.

Friedlingstein, P., O'Sullivan, M., Jones, M. W., Andrew, R. M., Hauck, J., Olsen, A., Peters, G. P., Peters, W., Pongratz, J., Sitch, S., Le Quéré, C., Canadell, J. G., Ciais, P., Jackson, R. B., Alin, S., Aragão, L. E. O. C., Arneth, A., Arora, V., Bates, N. R., Becker, M., Benoit-Cattin, A., Bittig, H. C., Bopp, L., Bultan, S., Chandra, N., Chevallier, F., Chini, L. P., Evans, W., Florentie, L., Forster, P. M., Gasser, T., Gehlen, M., Gilfillan, D., Gkritzalis, T., Gregor, L., Gruber, N., Harris, I., Hartung, K., Haverd, V., Houghton, R. A., Ilyina, T., Jain, A. K., Joetzjer, E., Kadono, K., Kato, E., Kitidis, V., Korsbakken, J. I., Landschützer, P., Lefèvre, N., Lenton, A., Lienert, S., Liu, Z., Lombardozzi, D., Marland, G., Metzl, N., Munro, D. R., Nabel, J. E. M. S., Nakaoka, S.-I., Niwa, Y., O'Brien, K., Ono, T., Palmer, P. I., Pierrot, D., Poulter, B., Resplandy, L., Robertson, E., Rödenbeck, C., Schwinger, J., Séférian, R., Skjelvan, I., Smith, A. J. P., Sutton, A. J., Tanhua, T., Tans, P. P., Tian, H., Tilbrook, B., van der Werf, G., Vuichard, N., Walker, A. P., Wanninkhof, R., Watson, A. J., Willis, D., Wiltshire, A. J., Yuan, W., Yue, X., and Zaehle, S.: Global Carbon Budget 2020, Earth System Science Data, 12, 3269-3340, 10.5194/essd-12-3269-2020, 2020.

Ge, Q. S., Dai, J. H., He, F. N., Pan, Y., and Wang, M. M.: Land use changes and their relations with carbon cycles over the past 300 a in China, Science China: Earth Sciences, 51, 871-884, 10.1007/s11430-008-0046-z, 2008.

Ge, Q. S., Dai, J. H., He, F. N., Zheng, J. Y., Man, Z. M., and Zhao, Y.: Spatiotemporal dynamics of reclamation and cultivation and its driving factors in parts of China during the last three centuries, Progress in Natural Science, 14, 605-613, 2004.

Hansis, E., Davis, S. J., and Pongratz, J.: Relevance of methodological choices for accounting of land use change carbon fluxes, Global Biogeochemical Cycles, 29, 1230-1246, 10.1002/2014gb004997, 2015.

Hartung, K., Bastos, A., Chini, L., Ganzenmüller, R., Havermann, F., Hurtt, G. C., Loughran, T., Nabel, J. E. M. S., Nützel, T., Obermeier, W. A., and Pongratz, J.: Bookkeeping estimates of the net land-use change flux-a sensitivity study with the CMIP6 land-use dataset, Earth System Dynamics, 12, 763-782, 10.5194/esd-12-763-2021, 2021.

He, F. N., Ge, Q. S., Dai, J. H., and Rao, Y. J.: Forest change of China in recent 300 years, Journal of Geographical Sciences, 18, 59-72, 10.1007/s11442-008-0059-8, 2008.

He, F., Li, S. C., Yang, F., and Li, M. J.: Evaluating the accuracy of Chinese pasture data in global historical land use datasets, Science China Earth Sciences, 61, 1685-1696, 10.1007/s11430-018-9256-1, 2018.

He, F., Li, S., and Zhang, X.: A spatially explicit reconstruction of forest cover in China over 1700-2000, Global and Planetary Change, 131, 73-81, 10.1016/j.gloplacha.2015.05.008, 2015.

He, F., Yang, F., and Wang, Y.: Reconstructing forest and grassland cover changes in China over the past millennium, Science China Earth Sciences, 67, 10.1007/s11430-024-1454-4, 2024.

He, F., Yang, F., Zhao, C., Li, S., and Li, M.: Spatially explicit reconstruction of cropland cover for China over the past millennium, Science China Earth Sciences, 66, 111-128, 10.1007/s11430-021-9988-5, 2023.

Heinimann, A., Mertz, O., Frolking, S., Egelund Christensen, A., Hurni, K., Sedano, F., Parsons Chini, L., Sahajpal, R., Hansen, M., and Hurtt, G.: A global view of shifting cultivation: Recent, current, and future extent, Plos One, 12, e0184479, 10.1371/journal.pone.0184479, 2017.

Houghton, R. A. and Castanho, A.: Annual emissions of carbon from land use, land-use change, and forestry from 1850 to 2020, Earth System Science Data, 15, 2025-2054, 10.5194/essd-15-2025-2023, 2023.

Houghton, R. A. and Hackler, J. L.: Sources and sinks of carbon from land-use change in China, Global Biogeochemical Cycles, 17, 1034, 10.1029/2002GB001970, 2003, 2003.

Houghton, R. A. and Nassikas, A. A.: Global and regional fluxes of carbon from land use and land cover change 1850–2015, Global Biogeochemical Cycles, 31, 456-472, 10.1002/2016gb005546, 2017.

Houghton, R. A., House, J. I., Pongratz, J., van der Werf, G. R., DeFries, R. S., Hansen, M. C., Le Quéré, C., and Ramankutty, N.: Carbon emissions from land use and land-cover change, Biogeosciences, 9, 5125-5142, 10.5194/bg-9-5125-2012, 2012.

Hurtt, G. C., Chini, L., Sahajpal, R., Frolking, S., Bodirsky, B. L., Calvin, K., Doelman, J. C., Fisk, J., Fujimori, S., Klein Goldewijk, K., Hasegawa, T., Havlik, P., Heinimann, A., Humpenöder, F., Jungclaus, J., Kaplan, J. O., Kennedy, J., Krisztin, T., Lawrence, D., Lawrence, P., Ma, L., Mertz, O., Pongratz, J., Popp, A., Poulter, B., Riahi, K., Shevliakova, E., Stehfest, E., Thornton, P., Tubiello, F. N., van Vuuren, D. P., and Zhang, X.: Harmonization of global land use change and management for the period 850–2100 (LUH2) for CMIP6, Geoscientific Model Development, 13, 5425-5464, 10.5194/gmd-13-5425-2020, 2020.

Jia, R., Fang, X., and Ye, Y.: Gridded reconstruction of cropland cover changes in Northeast China from AD 1000 to 1200, Regional Environmental Change, 23, 10.1007/s10113-023-02118-y, 2023.

Kabora, T. K., Stump, D., Thomas, C. D., and Beale, C. M.: Assessing inconsistencies in historical land-use reconstructions for Africa at 1800, Regional Environmental Change, 24, 10.1007/s10113-024-02224-5, 2024.

Kaplan, J. O., Ruddiman, W. F., Crucifix, M. C., Oldfield, F. A., Krumhardt, K. M., Ellis, E. C., Ruddiman, W. F., Lemmen, C., and Klein Goldewijk, K.: Holocene carbon emissions as a result of anthropogenic land cover change, The Holocene, 21, 775-791, 10.1177/0959683610386983, 2011.

Klein Goldewijk, K., Beusen, A., Doelman, J., and Stehfest, E.: Anthropogenic land use estimates for the Holocene - HYDE 3.2, Earth System Science Data, 9, 927-953, 10.5194/essd-9-927-2017, 2017.

Klein Goldewijk, K.: Estimating global land use change over the past 300 years: The HYDE Database, Global Biogeochemical Cycles, 15, 417-433, 10.1029/1999GB001232, 2001.

Li, B. B., Fang, X. Q., Y, Y., and Zhang, X. Z.: Carbon emissions induced by cropland expansion in Northeast China during the past 300 years, Science China: Earth Sciences, 57, 2259-2268, 2014.

Li, M. J., He, F. N., Li, S. C., and Yang, F.: Reconstruction of the cropland cover changes in eastern China between the 10(th) century and 13(th) century using historical documents, Scientific Reports, 8, 13552, 10.1038/s41598-018-31807-6, 2018a.

Li, M. J., He, F. N., Yang, F., and Li, S. C.: Reconstructing provincial cropland area in eastern China during the early Yuan Dynasty(AD1271-1294), Journal of Geographical Sciences, 28, 1994-2006, 10.1007/s11442-018-1576-8, 2018b.

Li, M., He, F., Yang, F., and Zhao, L.: Reconstruction of provincial cropland area and its spatial-temporal characteristics in

the Ming Dynasty, Geographical research, 39, 447-460, 10.11821/dlyj020181315, 2020.

Li, S. C., He, F. N., and Zhang, X. Z.: A spatially explicit reconstruction of cropland cover in China from 1661 to 1996, Regional Environmental Change, 16, 417-428, 10.1007/s10113-014-0751-4, 2016.

Mendelsohn, R. and Sohngen, B.: The net carbon emissions from historic land use and land use change, Journal of Forest Economics, 34, 263-283, 10.1561/112.00000505, 2019.

Obermeier, W. A., Schwingshackl, C., Bastos, A., Conchedda, G., Gasser, T., Grassi, G., Houghton, R. A., Tubiello, F. N., Sitch, S., and Pongratz, J.: Country-level estimates of gross and net carbon fluxes from land use, land-use change and forestry, Earth System Science Data, 16, 605-645, 10.5194/essd-16-605-2024, 2024.

Pongratz, J., Reick, C. H., Raddatz, T., and Claussen, M.: Effects of anthropogenic land cover change on the carbon cycle of the last millennium, Global Biogeochemical Cycles, 23, GB4001, 10.1029/2009gb003488, 2009.

Pongratz, J., Reick, C., Raddatz, T., and Claussen, M.: A reconstruction of global agricultural areas and land cover for the last millennium, Global Biogeochemical Cycles, 22, GB3018, 10.1029/2007gb003153, 2008.

Qin, Z., Zhu, Y., Canadell, J. G., Chen, M., Li, T., Mishra, U., and Yuan, W.: Global spatially explicit carbon emissions from land-use change over the past six decades (1961–2020), One Earth, 7, 1-13, 10.1016/j.oneear.2024.04.002, 2024.

Ramankutty, N. and Foley, J. A.: Estimating historical changes in global land cover: Croplands from 1700 to 1992, Global Biogeochemical Cycles, 13, 997-1027, 10.1029/1999GB900046, 1999.

Soil Species of China. Volume 1-6. Beijing: China Agriculture Press, 1995.

Wedderburn-Bisshop, G.: Deforestation—a call for consistent carbon accounting, Environmental Research Letters, 19, 111006, 10.1088/1748-9326/ad7d21, 2024.

Wei, X., Ye, Y., Li, B., and Chen, T.: Reconstructing cropland change since 1650 AD in Shaanxi province, central China, Quaternary International, 641, 74-86, 10.1016/j.quaint.2022.02.025, 2022.

Winkler, K., Yang, H., Ganzenmüller, R., Fuchs, R., Ceccherini, G., Duveiller, G., Grassi, G., Pongratz, J., Bastos, A., Shvidenko, A., Araza, A., Herold, M., Wigneron, J.-P., and Ciais, P.: Changes in land use and management led to a decline in Eastern Europe's terrestrial carbon sink, Communications Earth & Environment, 4, 237, 10.1038/s43247-023-00893-4, 2023.

Xu, L., He, N., and Yu, G.: A dataset of carbon density in Chinese terrestrial ecosystems (2010s), China Sci. Data 4, 49-54, 2019.

Yang, F., Dong, G., Meng, X., Gao, Y., He, F., Li, M., Li, W., Liu, Z., Zhai, X., Wu, P., Zhang, H., Mao, Q., Yao, Y., and Yue, C. Annual carbon emissions from land use change in China from 1000 to 2019 [Data set]. Zenodo. https://doi.org/10.5281/zenodo.14557386, 2025.

Yang, F., He, F. N., Li, M. J., and Li, S. C.: Evaluating the reliability of global historical land use scenarios for forest data in China, Journal of Geographical Sciences, 30, 1083-1094, 10.1007/s11442-020-1771-2, 2020.

Yang, F., He, F., Li, S., Li, M., and Wu, P.: A new estimation of carbon emissions from land use and land cover change in China over the past 300 years, Science of The Total Environment, 863, 160963, 10.1016/j.scitotenv.2022.160963, 2023.

Yang, X., Jin, X., Xiang, X., Fan, Y., Liu, J., Shan, W., and Zhou, Y.: Carbon emissions induced by farmland expansion in China during the past 300 years, Science China Earth Sciences, 62, 423–437, 10.1007/s11430-017-9221-7, 2019.

Yang, X., Jin, X., Xue, Q., and Zhou, Y.: Reconstruction of the spatial distribution of historical farmland in the Taiwan Province of China for 1659-1945, Land Use Policy, 114, 105951, 10.1016/j.landusepol.2021.105951, 2022.

Yang, Y., Mohammat, A., Feng, J., Zhou, R., Fang, J.: Storage, patterns and environmental controls of soil organic carbon in China, Biogeochemistry, 84, 131-141, 2007.

Ye, Y., Fang, X. Q., Ren, Y. Y., Zhang, X. Z., and Chen, L.: Cropland cover change in Northeast China during the past 300 years, Science China Earth Sciences, 52, 1172-1182, 10.1007/s11430-009-0118-8, 2009.

Yu, Z., Ciais, P., Piao, S., Houghton, R. A., Lu, C., Tian, H., Agathokleous, E., Kattel, G. R., Sitch, S., Goll, D., Yue, X., Walker, A., Friedlingstein, P., Jain, A. K., Liu, S., and Zhou, G.: Forest expansion dominates China's land carbon sink since 1980, Nat Commun, 13, 5374, 10.1038/s41467-022-32961-2, 2022.

Yu, Z., Jin, X., Miao, L., and Yang, X.: A historical reconstruction of cropland in China from 1900 to 2016, Earth System Science Data, 13, 3203-3218, 10.5194/essd-13-3203-2021, 2021.

Yue, C., Ciais, P., Houghton, R. A., and Nassikas, A. A.: Contribution of land use to the interannual variability of the land carbon cycle, Nat Commun, 11, 3170, 10.1038/s41467-020-16953-8, 2020.

Yue, C., Xu, M., Ciais, P., Tao, S., Shen, H., Chang, J., Li, W., Deng, L., He, J., Leng, Y., Li, Y., Wang, J., Xu, C., Zhang, H., Zhang, P., Zhang, L., Zhao, J., Zhu, L., and Piao, S.: Contributions of ecological restoration policies to China's land carbon balance, Nat Commun, 15, 9708, 10.1038/s41467-024-54100-9, 2024.

Zhao, C., He, F., Yang, F. and Li, S.: Uncertainties of global historical land use scenarios in past-millennium cropland reconstruction in China, Quaternary International, 641, 87-96, 10.1016/j.quaint.2022.03.020, 2022.